

Atmospheric oxidation of unsaturated hydrofluoroethers initiated by OH radicals

Maissa A. Adi, Mohammednoor Altarawneh*

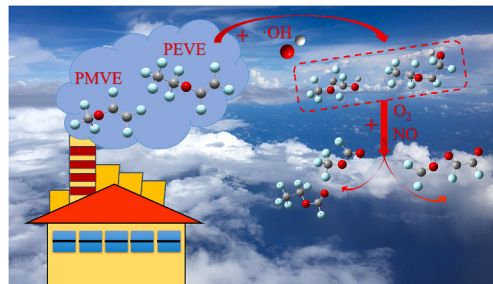
Department of Chemical and Petroleum Engineering, United Arab Emirates University, Sheikh Khalifa bin Zayed Street, Al-Ain, United Arab Emirates



HIGHLIGHTS

- The study investigates atmospheric oxidation of two hydrofluoroethers (HFEs) model compounds.
- Reaction mechanisms were mapped out to underpin the governing atmospheric removal of HFEs.
- The developed kinetic model illustrates time-dependent profiles of the major experimental products.
- Atmospheric lifetimes of HFEs are found to be sensitive to the length of the carbon chain.
- The analysis of absolute rate of production portrays the most important reactions.

GRAPHICAL ABSTRACT



ARTICLE INFO

Keywords:
Hydrofluoroethers
Atmospheric oxidation
OH radicals
Reaction mechanism
Kinetic model

ABSTRACT

Hydrofluoroethers (HFEs) are perfluorinated chemicals that were developed as alternative for chlorofluorocarbons (CFCs) in various applications. Among notable unsaturated HFEs are perfluoro methyl vinyl ether (PMVE, $\text{CF}_3\text{OCF}=\text{CF}_2$) and perfluoro ethyl vinyl ether (PEVE, $\text{C}_2\text{F}_5\text{OCF}=\text{CF}_2$). During the implementation of PMVE and PEVE, they spill and release to the atmosphere. Due to the tendency of perfluorinated compounds to have strong infrared absorption features and long atmospheric lifetimes, they are among the most potent greenhouse gases. Thus, it is important to accurately assess their atmospheric sink routes in order to assess their impact on climate change. Herein, we illustrated detailed mechanistic pathways and developed kinetic models with the underlying aim to comprehend the atmospheric fate of the title HFEs and the likely products of decomposition. It was found that the production of main products to stem from the addition of OH radical to the inner carbon-carbon double bond atoms. Atmospheric lifetimes of PMVE and PEVE were calculated to be ~23 and ~56 h; respectively. Time-dependent molar yields are acquired for the experimentally major products; namely carbonyl fluoride (CF_2O), perfluorinated glyoxal (CFOCFO), perfluorinated methylformates (CF_3OCFO and $\text{CF}_3\text{CF}_2\text{OCFO}$). Photochemical Ozone Creation Potentials (POCPs) of PMVE and PEVE were calculated to be 1.78 and 1.18, respectively. Obtained results tap into efforts that aim to understand the atmospheric chemistry cycles of perfluorinated chemicals in general.

* Corresponding author.

E-mail address: mn.altarawneh@uaeu.ac.ae (M. Altarawneh).

List of abbreviations

(HFEs)	Hydrofluoroethers
(CFCs)	Chlorofluorocarbons
(HFCs)	Hydrofluorocarbons
(PFCs)	Perfluorinated compounds
(PFASs)	Polyfluoroalkyl substances
(MVE)	Methyl vinyl ether
(PPVE)	Propyl vinyl ether
(PFOA)	Perfluorooctanoic acid
(PFOS)	Perfluorooctanesulfonic acid
(PMVE)	Perfluoro methyl vinyl ether
(PEVE)	Perfluoro ethyl vinyl ether
(DFT)	Density functional theory
(POCP)	Photochemical Ozone Creation Potential

in reference to HFCs. It is of importance to investigate the atmospheric chemistry of HFEs since they are capable to absorb light in the IR region, and thus contributing to global warming (Good and Francisco, 2003). The prime aim is to ascertain the likely impact of their decomposed products, and to reveal the governing reaction mechanisms. For instance, atmospheric decomposition of HFEs produces trifluoroacetic acid CF_3COOH as a major product (Holland et al., 2021). CF_3COOH is a potent green-house gas (GHG) (Shohrat et al., 2022). Pertinent experimental and (Orkin et al., 2011) theoretical work (Lily et al., 2021) has focused on initiation reactions by OH, Cl, and NO_x species, in case of the presence of abstractable H atoms in the structures of HFEs. Detected products by spectroscopic techniques along with density functional theory (DFT) calculations assisted in the construction of representative reaction mechanisms.

Perfluoro (methylene vinyl ether) (PMVE, $\text{CF}_3\text{OCF}=\text{CF}_2$) and perfluoro (ethyl vinyl ether) (PEVE, $\text{C}_2\text{F}_5\text{OCF}=\text{CF}_2$) are classified as unsaturated perfluoro HFEs. Both compounds tend to release to the atmosphere during their implementation in the production of perfluorinated polymers and (Zharov and Nikolaeva, 2010) in plasma etching operations (Kondo et al., 2015). Unlike HFCs, the absence of an abstractable hydrogen atoms along with the presence of the unsaturated $\text{C}=\text{C}$ bond affords distinct atmospheric degradation pathways for PMVE and PEVE. As illustrated by Bunkan et al. (2018), OH addition to the double bonds commences the atmospheric degradation of PEVE; mainly into CF_2O , CF_3OCFO , and CFOCFO (at 1–50 Torr). At 1 atm, formation of a considerable amount of perfluoro glyoxal, CFOCFO (Vereecken et al., 2015) was attributed to conversion of fluorinated glycolaldehyde to perfluoro glyoxal catalyzed by the elevated concentrations of H_2O and $(\text{H}_2\text{O})_2$ in atmosphere. Initial reactions of PEVE with OH entails negative activation energy (Gonu et al., 2018). Computed reaction rate constants ($\sim 3 \times 10^{-12} \text{ cm}^3 \text{ molecule}^{-1} \text{ s}^{-1}$) reflected that PEVE can prolong in the atmosphere for a few days (Srinivasulu et al., 2018). In atmospheric oxidation of PEVE, the presence of NO_x and HO_2 radicals promotes the consumption of the initially formed peroxy radicals into carbonyl fluoride CF_2O . Other detected products by FTIR included $\text{C}_2\text{F}_5\text{OCFO}$ and CFOCFO at relatively low yields. Hydrolysis reactions of CF_2O is expected to yield CO and HF. As observed in the atmospheric oxidation of FTOH (Altarawneh, 2021a,b), the concentration of NO_x altered the products distributions from the oxidation of PEVE (Srinivasulu et al., 2018). The atmospheric oxidation of the shorter PMVE molecule ensues via similar mechanistic profiles as described by Mashino et al. (2000). Atmospheric oxidation at 700 Torr predominantly produced CF_2O , CF_3OCOF , and CFOCFO . Vereecken et al. (2015) utilized DFT calculations to compute reaction and activation energies that features the atmospheric oxidation of PMVE. However, their study did not compile the constructed mechanism into a representative kinetic model.

In this study, we build on the mechanisms presented by Bunkan et al. (2018) (PEVE), Mashino et al. (2000) and Vereecken et al. (2015) (PMVE), to construct a kinetic model that accounts for the salient features underpinning atmospheric oxidation of these two unsaturated HFEs compounds. The aim of the formulated kinetic model is twofold; to illustrate pathways for the formation of major experimentally products, and to accurately calculate the lifetimes of HFEs under real atmospheric scenarios. These conditions entail deploying typical concentrations of reactive species (parent HFEs, OH, and NO) at the ambient conditions. Accruing this information will assist in determining atmospheric fate of PMVE and PEVE and the potential hazard of their degradation once released.

2. Computational details

The hybrid meta density functional theory (M06–2X DFT) associated with the basis set 6–311 + G(d,p) (Montgomery et al., 2000) was deployed to map out reactions mechanisms and to compute vibrational frequencies; as implemented in the Gaussian16 code (Frisch et al., 2016). In case of perfluorinated compounds, we have recently found that

1. Introduction

Owing to their unique physiochemical properties (high thermal stability and low-surface reactivity), perfluorinated compounds (PFCs), most notably, polyfluoroalkyl substances (PFASs), have been used over the last five decades in a multitude of applications (McDonough et al., 2022). These applications span coating materials, fire-fighting foams, lubricants, and packaging. Generally, PFCs compounds have been associated with adverse health and environmental effects (Cousins et al., 2020). For examples, it has been well-established that certain congeners induce several types of cancer (Glüge et al., 2020). Depending on the deployed functional group, PFASs are categories into ionic, *i*-PFASs (such as carboxylic (PFCAs) and sulfonic acids (PFOSSs), and neutral compounds, *n*-PFASs (such as fluorotelomer alcohols, FTOHs). The hydrophilic functional groups in the *i*-PFASs family render these compounds to be widely distributed in the aquatic environment (Cousins et al., 2020). On the contrary, *n*-PFASs compounds are volatile species and mainly exist in the gas phase. The latter compounds undergo long-range atmospheric transports. This phenomenon might explain the presence of FTOHs in remote areas such as the arctic regions. Furthermore, atmospheric oxidation of FTOHs is regarded as a potential source for the observed high yields of PFCAs that exceeds pertinent emission profiles (Ellis et al., 2004). For instance, it is estimated that ~25% of FTOHs load in the atmosphere is converted into PFCAs whereas 4% is deposited as the notorious perfluorooctanoic acid (PFOA) (Thackray et al., 2020). Therefore, simultaneous analysis of *n*-PFASs and *i*-PFASs in the atmosphere helps to understand their sources and transport. Due to the toxic nature and their tendency for bioaccumulation, production of several isomers of PFASs has been gradually phased out in many parts of the world (Sunderland et al., 2019).

In addition to ocean currents, atmospheric pathways remain the chief routes for the degradation, transportation and transformation of PFCs (Cheng et al., 2021). When compared with other environmental matrices, the atmospheric environment signifies an important exposure compartment for the effect of PFCs on humans and living organisms (Wang et al., 2022). For this reason, understanding the atmospheric chemistry of PFCs is important to comprehend their environmental distributions, to illustrate their likely transformation pathways, and to quantify their environmental loads.

Along the same line of enquiry, hydrofluoroethers (HFEs) are a class of PFCs that was developed as an alternative to the ozone-depleting agents of hydrofluorocarbons (HFCs) and chlorofluorocarbons (CFCs) (Jovell et al., 2022). The facile release of chlorine atoms from the latter group via photodegradation initiates a chain of reactions that consume the atmospheric ozone (Yu et al., 2022). The presence of the relatively weak ether linkage in HFEs compounds enhances their atmospheric degradation (Lily et al., 2020), and hence they endure shorter lifetimes

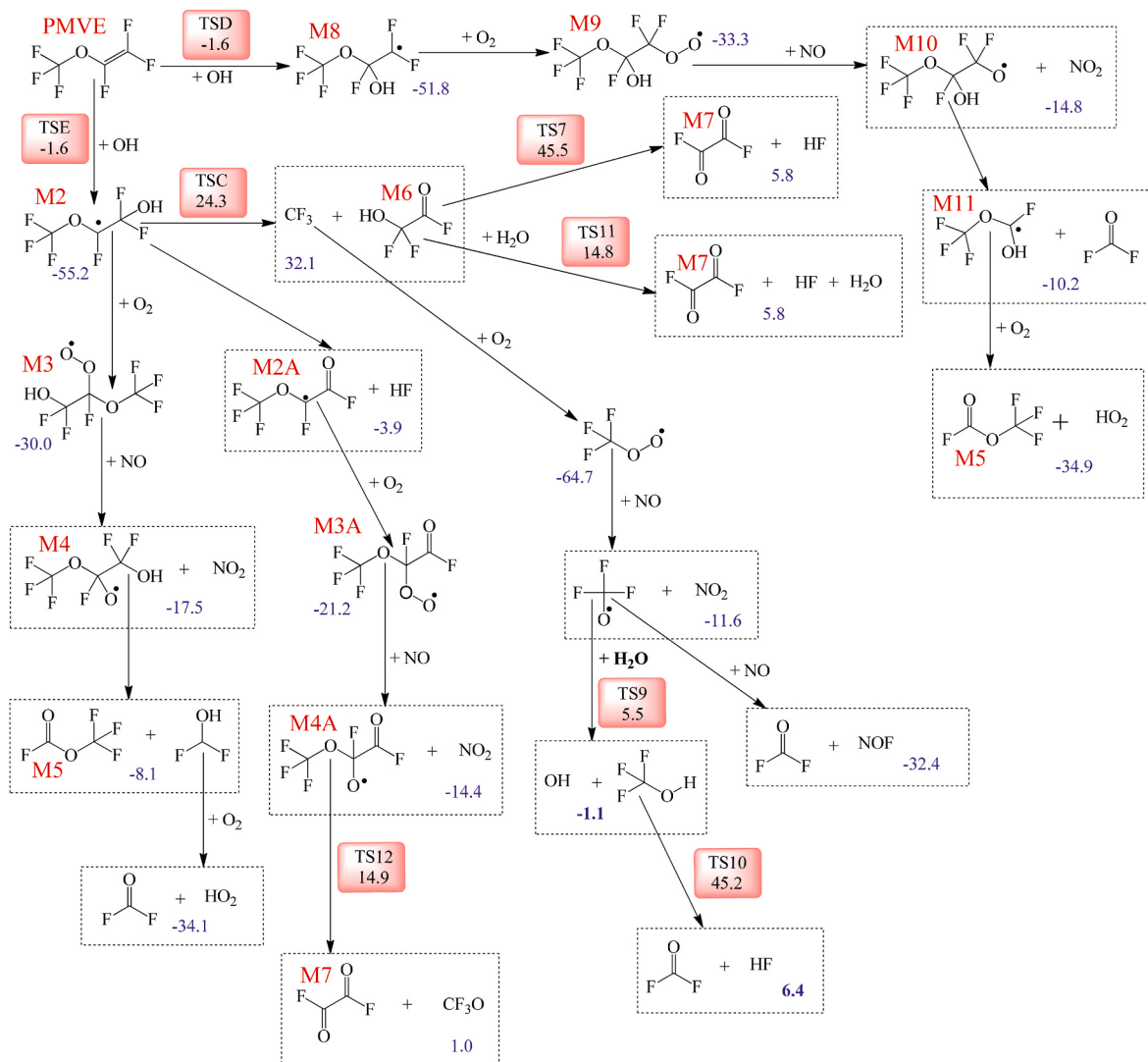


Fig. 1. PMVE's atmospheric oxidation initiated by OH pathways. Values are in kcal/mol at 298.15 K. Values in blue, and inside red box represent reaction enthalpies and activation enthalpies; respectively.

bond dissociation energies obtained at the M062X level to depart by 1–2 kcal/mol (Altarawneh, 2021a,b) in reference to values calculated using the computationally more demanding chemistry models such as WIU and CBS-APNO (Purnell et al., 2018). Likewise, a close agreement between experimental and DFT-calculated reaction rate constant confirms the suitability of the M062X method for the application at hand (Altarawneh et al., 2009, 2013; Altarawneh, 2021a,b). A similar conclusion was also attained by Khan et al. (2020). The M06-2X functional was parametrized against a large set of experimental and high-level theoretical data to satisfactorily perform in acquiring thermo-kinetic data and to accurately describe systems that involve long-range interactions (Zhao and Truhlar, 2008). The designated reaction pathway was confirmed via performing intrinsic reaction coordinates (IRC) calculations. Reaction enthalpies ($\Delta_{rxn} H^\circ_{298.15}$) and the activation barriers ($\Delta_{rxn}^# H^\circ_{298.15}$) illustrated in Fig. 2 and Fig. 4, were calculated based on the following formula:

$$\Delta_{rxn} H^\circ_{298.15} = \Sigma n \dot{H}_{298.15}^\circ (products) - \Sigma n \dot{H}_{298.15}^\circ (reactants)$$

$$\Delta_{rxn}^# H^\circ_{298.15} = \Sigma n \dot{H}_{298.15}^\circ (transition\ state) - \Sigma n \dot{H}_{298.15}^\circ (reactants)$$

whereas, values of activation barriers (E_a) shown in Table 2, were computed by the KiSTheLP software (Canneaux et al., 2014) through fitting of the Arrhenius parameters: $k(T) = A \exp(-E_a/RT)$. Values of

$\Sigma n \dot{H}_{298.15}^\circ (products)$, $\Sigma n \dot{H}_{298.15}^\circ (reactants)$, and $\Sigma n \dot{H}_{298.15}^\circ (transition\ state)$ are obtained from the Gaussian 16 software.

In atmospheric reactions, the temperature range of interests typically extends between 260 and 320 K (Altarawneh, 2021a,b). In order to find the NASA polynomials such as temperature-dependent thermochemical characteristics: enthalpy of formation, heat capacity and standard entropy, the ChemRate software (Mokrushin et al., 2002) was implemented based on the calculated standard enthalpies of formation ($\Delta H_f^\circ_{298}$) of species, rotational constants, and vibrational frequencies. More details on the performed procedures can be found in recent studies (Altarawneh, 2022; Razmgar et al., 2022). Isodesmic-work reactions estimated values of $\Delta H_f^\circ_{298}$ for PMVE and PEVE molecules to be −361.8 and −458.7 kcal/mol, respectively. Considering a batch reactor model to simulate the atmospheric environment, the Chemkin-Pro package executes kinetic modelling at 298.15 K with actual time ranging between 1.0 and 1400 min. Thermo-kinetic parameters of the model and Cartesian Coordinates for all species are provided in the Supplementary Material (SM).

3. Results and discussions

Two main pathways were explored for the atmospheric oxidation of PMVE and PEVE, through which the OH radical plays the role of the

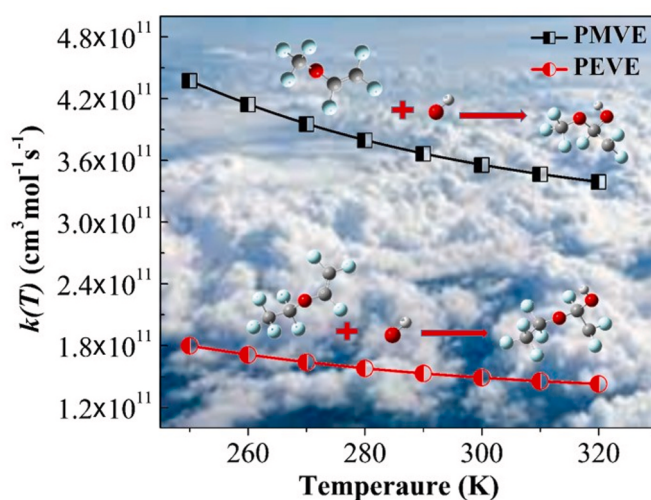


Fig. 2. Reaction rate constants of the addition of OH to the inner carbon atoms in PMVE and PEVE molecules, between 250 and 320 K.

reaction's initiator. Atmospheric oxidation pathways commence with the addition of OH radicals to the outer and inner double C=C bonds in both molecules, and thus, opening up two distinct pathways. Using the generated kinetic models, carbonyl fluoride (CF₂O) appears as the main product, followed by perfluoro glyoxal (CFOCFO). Appreciable loads CF₃OCFO and CF₃CF₂OCFO were also detected from the atmospheric oxidation of PMVE and PEVE. Formation of these products was also confirmed experimentally for the atmospheric oxidation of PMVE and PEVE initiated by OH radical (Li et al., 2000; Mashino et al., 2000; Bunkan et al., 2018).

3.1. Mechanism of OH-initiated atmospheric oxidation of perfluoro methyl vinyl ether, (PMVE)

The degradation mechanism of PMVE as illustrated in Fig. 1, proceeds via two main OH addition channels, to the double bond of the outer carbon and to the inner carbon atom through the transition states TSE and TSD, respectively. Reaction barriers for these two transition states reside below the separated reactants by -1.5 kcal/mol. This value matches previously estimated figure by Vereecken et al. (2015) where the rate coefficient exhibits a negative temperature dependency. As in atmospheric reactions, it is likely that a pre-reactant OH complex initially forms, and hence transition state for the OH addition reactions resides above this complex (Altarawneh, 2021a,b). Fig. 2 shows variation of reaction rate constants for OH addition to the inner carbon atom in both molecules between 250 and 320 K.

Considering the perfluoro propyl vinyl ether (PPVE) molecule, addition of OH to the terminal atom of the carbon-carbon double bond was found to be the predominant channel in reference to addition to the inner carbon atom of the C=C double bond (Amedro et al., 2015). Similarly, it was found experimentally that during photo-oxidation of PEVE initiated by OH radicals, the product flux proceeds through addition of OH to the outer carbon atom (Bunkan et al., 2018). Our computed reaction enthalpies for addition of OH to the outer and to the inner carbon atoms in the PMVE molecule entail values of -55.2 kcal/mol and -51.8 kcal/mol forming the adducts M2 and M8, respectively. These values match very well previously corresponding values reported by Vereecken et al. (2015) at -54 kcal/mol and -52 kcal/mol. OH addition pathways to the analogous non-fluorinated compound methyl vinyl ether, were found to be considerably less exothermic in the range of 33–44 kcal/mol (Sun et al., 2008). Such discrepancy stems from the nature of fluorine atoms as electron withdrawing groups that facilitate addition of OH to the carbon cut.

In a study by Sun et al. (2008) on the photo-oxidation of methyl vinyl

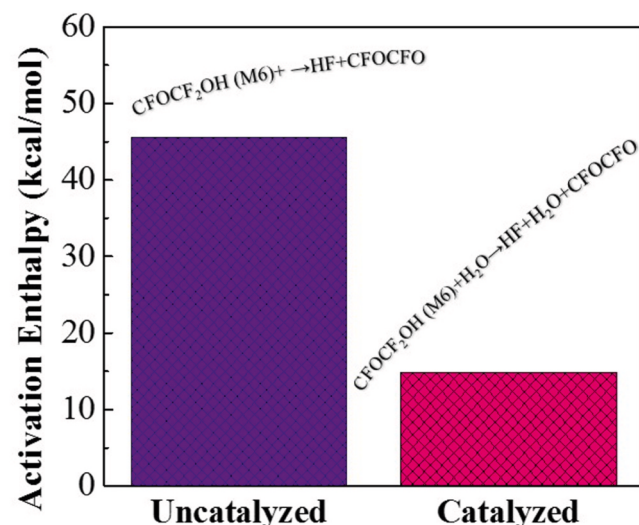


Fig. 3. Activation enthalpy of the uncatalyzed and water-catalyzed reactions that operate in the production of CFOCFO.

ether (MVE), the adduct CH₃CHOCH₂OH, the non-fluorinated analogous of M2, can dissociate via an unimolecular reaction or react with atmospheric oxygen molecules. Analogously and as Fig. 1 depicts, the adduct M2 branches into three channels. The first pathway features elimination of HF forming the intermediate M2A in a slightly exothermic reaction. Despite of our best efforts, we were unable to locate a transition state for this reaction. The same reaction channel was also suggested by other studies on the atmospheric oxidation of PMVE (Li et al., 2000; Mashino et al., 2000; Vereecken et al., 2015). The M2A adduct then reacts with ambient oxygen molecules to produce M3A peroxy radical that ultimately forms M4A through peroxy'O abstraction by NO. The later moiety dissociates through an endothermic reaction (1.0 kcal/mol) to produce CF₃O and the experimentally detected perfluoro glyoxal CFOCFO (M7) with a relatively sizable barrier of 14.9 kcal/mol (TS12). The latter value matches a previously obtained value at 18 kcal/mol (Vereecken et al., 2015).

The second dissociation path results in the formation of fluorinated glycolaldehyde CFOCFOH (M6) and CF₃ with an enthalpic barrier of 24.3 kcal/mol (TSC); a value that matches very well a corresponding value reported for the same reactive system of PMVE + OH at 24 kcal/mol (Vereecken et al., 2015). Addition of O₂ to CF₃ radical is highly exothermic at 64.7 kcal/mol and produces CF₃O₂. This reaction typically prevails in the atmospheric oxidation of perfluorinated compounds where CF₃O₂ serves as precursor in the formation of carbonyl fluoride via bimolecular reactions that involve NO and H₂O (Mashino et al., 2000; Altarawneh, 2021a,b). Several studies reported that, the adduct CF₃O under atmospheric conditions, reacts with either NO_x leading to the production of CF₂O, or with hydrocarbons producing CF₃OH (Jensen et al., 1994; Kelly et al., 1994; Turnipseed et al., 1995; Wallington and Ball, 1995; Andersen and Nielsen, 2022). Following a rapid reaction between NO and CF₃O (Jensen et al., 1994; Mashino et al., 2000; Brudnik et al., 2011), products such as NOF and CF₂O may also be formed at the enthalpic barrierless value of -32.4 kcal/mol. Formation of NOF was detected via the same later reaction channel in a multi-photon infrared decomposition of CF₃OOCF₃ (Li and Francisco, 1991).

As Fig. 1 shows, the reaction of water with CF₃O radical, produces CF₃OH via enthalpic energy of 5.5 kcal/mol through TS9. In view of the very sizable barrier of TS10 (45.2 kcal/mol), it is unlikely that carbonyl fluoride to arise from CF₃OH. Likewise, it is unfeasible to form CFOCFO via unimolecular elimination of HF from M6 in view of the high enthalpic activation 45.4 kcal/mol embedded in TS7. Alternatively, the formation of CFOCFO is expected to be through a water-catalyzed reaction via a barrier of only 14.8 kcal/mol (TS11). Fig. 3 contrasts energy

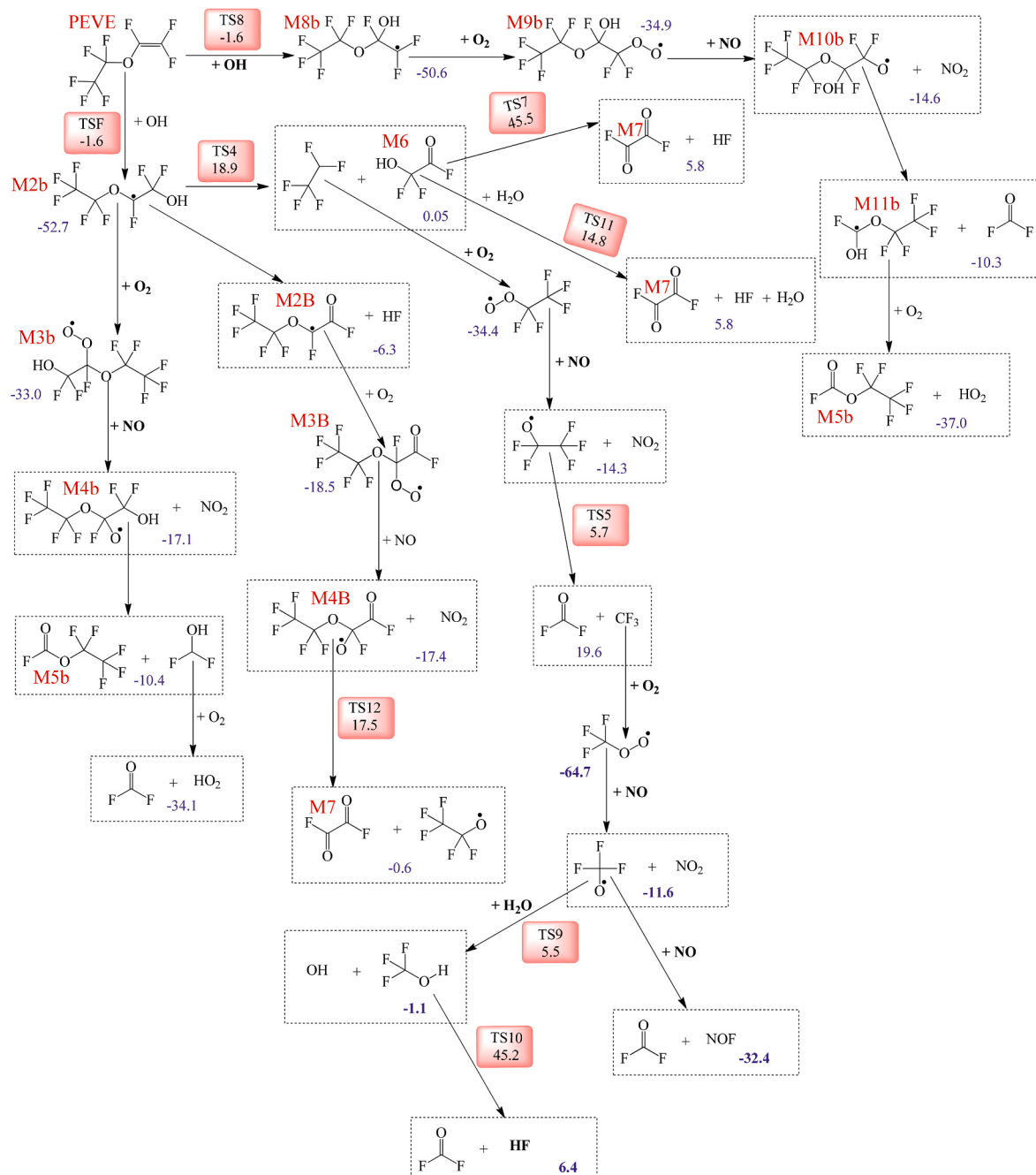


Fig. 4. PEVE's atmospheric oxidation by OH pathways. Values are in kcal/mol at 298.15 K. Values in blue, inside red box represent reaction enthalpies and activation enthalpies; respectively.

requirements for these two pathways. These two reaction pathways were also highlighted by Vereecken et al. (2015) with well-matched corresponding enthalpic barriers.

A great deal of work focused on the role of water as a catalyst in the elimination of HF from CF_3OH utilizing the simpler molecule $\text{CFOC-F}_2\text{OH}$ (Brudnik et al., 2008; Buszek and Francisco, 2009; Long et al., 2010; Brudnik et al., 2011; Saheb and Pourhaghghi, 2014; Ding et al., 2022). This type of reaction aids to understand the experimental rapid consumption of CF_3OH . Moreover, a self-catalyzed reaction may have contributed in the consumption of CF_3OH molecule (Nguyen et al., 2008).

The third reaction channel that involves M2 as a reactant is an oxidation reaction which represents the most energetically feasible channel among the suggested dissociation paths of M2. Under

atmospheric conditions and in accordance with the experimental observations, the moiety $\text{CF}_3\text{OCFCF}_2\text{OH}$ (M2) can be stabilized by oxidation reaction producing the peroxy radical $\text{CF}_3\text{OCFO}_2\text{CF}_2\text{OH}$ (M3) (Mashino et al., 2000). This was followed by the reaction between the later peroxy radical and NO resulting in the formation of the oxygen-centered radical $\text{CF}_3\text{OCFOCF}_2\text{OH}$ (M4) and NO_2 . The formed oxy radical undergoes carbon–carbon bond scission producing CF_3OCFO (M5) and CF_2OH radical. Following that, an oxidation reaction between CF_2OH radical and O_2 ensues rapidly resulting in the formation of F_2CO and HO_2 . Inspection of reaction pathways shown in Fig. 1 indicates that OH addition to the outer carbon atom to produce C_2FO and CFOCFO molecules. As depicted in the uppermost part of Fig. 1, addition of OH to the inner carbon atom produces M5 and CF_2O molecules in a series of reactions that are derived by atmospheric NO. The final reaction

signifies H abstraction from the hydroxyl group in M11 by atmospheric oxygen molecules, without encountering a reaction barrier.

3.2. Mechanism of OH-initiated atmospheric oxidation of perfluoro ethyl vinyl ether (PEVE)

The suggested mechanistic pathways for the atmospheric oxidation PEVE initiated by OH, as shown in Fig. 4, follows alike steps to these portrayed in Fig. 1 for the PMVE molecule. Addition of OH to the inner and outer carbon atom at the double C=C moiety entails negative activation barriers of 1.6 kcal/mol and results in the formation of the M8b and M2b intermediates; respectively. Similar to the case of PMVE, illustrated routes lead to the formation of CF₂O and CF₃CF₂OCFO (M5b). As Fig. 4 presents, these pathways commence with the reaction of the initially formed peroxy adduct with NO followed by C–C bond fission. It is generally viewed that OH addition to the outer carbon atoms in the double bond of HEFs kinetically dominate over addition at the inner carbon atom (Bunkan et al., 2018).

Pathways shown in Fig. 4 leads to the synthesis of the CF₂O, three major experimental products CF₂O, CF₃CF₂OCFO (M5b) and CFOCFO as demonstrated by Bunkan et al. (2018). Molecular oxygen adds to the apparent radical site in the initially formed M2b to form the adduct M3b. The latter reacts with atmospheric NO to produce the M4b intermediate. M5b forms through fission of a C–C bond in a reaction that also forms CF₂OH. H abstraction from the hydroxyl'H in the latter forms CF₂O in an exothermic reaction of 34.1 kcal/mol. In an alternative pathway, unimolecular dissociation of M2b through TS4 opens pathways for the formation of CFOCFO and F₂O. TS4 characterizes the formation of CF₃CF₂ radical and M6 molecule in a thermodynamically neutral reaction. These reactions ensue in an analogy to those illustrated in the previous section for the PMVE molecule. A series of oxygen addition reactions and bimolecular reactions with NO convert the CF₃CF₂ radical into two CF₂O molecules as the middle part of Fig. 4 shows. The CF₃CF₂O decomposes rapidly due to its thermal instability forming CF₂O and CF₃ (Giessing et al., 1996; Sornitz and Zellner, 2001). Further reactions occurred to the CF₃ radical with O₂ and NO producing CF₂O. Involved reactions are highly exothermic and proceed with facile activation barriers. While we were not able to locate a transition state for the HF elimination from M2b into M2B, we envisage that this reaction could be catalyzed by other atmospheric species; most notably water and CH₃O. Further atmospheric oxidation of M3B forms CFOCFO and CF₂O. The former could also originate from water elimination from M6 through a modest reaction barrier of 14.8 kcal/mol (TS11). As it is the case for the PMVE molecule; water-assisted elimination of HF via TS11 provides a facile pathway for the formation of the important product CFOCFO. As shown in the upper part of Fig. 4, oxygen addition to the radical site in the M8b intermediate results ultimately in the formation of M5B and CF₂O in a series of reactions that involve atmospheric O₂/NO species. In the light of the above, it can be stated that, the proposed path after TS4 in the PEVE mechanism is more complex when compared with the analogous one (TSC) in the PMVE. This is due to the difference in the produced intermediate, which is C₂F₅ (via TS4) in the case of PEVE, while it is CF₃ (via TSC) for PMVE. However, the suggested mechanism for both PEVE and PMVE consists of the same four reaction categories which will be mentioned in the following section (3.2).

3.3. Kinetic models of OH-initiated atmospheric oxidation of PMVE and PEVE

3.3.1. Time-dependent profiles of products

To the best of our knowledge, literature presents no study that investigated and illustrated (via computational kinetic model) atmospheric oxidation of unsaturated HEFs initiated by OH. As highlighted in the Introduction, experimental decay profiles pertinent to atmospheric oxidation of PEVE were reported by Bunkan et al. (2018). Thus, it is insightful to construct kinetic models for the atmospheric removal of

Table 1
Molar fraction of the species as executed using Chemkin-Pro package.

Species	Molar fraction	Reference
CF ₃ OCF=CF ₂ (PVME)	1.64 × 10 ⁻¹⁷	Bunkan et al. (2018)
C ₂ F ₅ OCF = CF ₂ (PEVE)	1.64 × 10 ⁻¹⁷	
H ₂ O	0.50 × 10 ⁻²	Thackray and Selin (2017)
HO ₂	1.48 × 10 ⁻¹⁷	
N ₂	0.78	
NO	3.27 × 10 ⁻¹⁰	
O ₂	0.21	
OH	3.27 × 10 ⁻¹²	

PMVE and PEVE initiated by OH with the capacity to account for the formation of the experimentally observed products CF₂O, CFOCFO, CF₃OCFO and CF₃CF₂OCFO, in addition to HF.

To predict product's profile for the atmospheric oxidation of the two considered HEFs, a batch reactor model was utilized to execute the kinetic simulations considering a volume of 1 m³, 1 atm pressure and at 298.15 K as temperature. Input to the model are the derived thermo-kinetic parameters from DFT calculations (as described in Section 2) in addition to the initial typical concentration in the atmosphere of the reactive species as enlisted in Table 1. The data are not available for the atmospheric loads of PVME and PEVE. For that reason, we have assumed their atmospheric concentrations to match that of other PFASs compounds, such as FTOH (Altarawneh, 2021a,b). Concentrations for the atmospheric species NO, HO₂ and OH follow their well-established loads in urban environment (Thackray and Selin, 2017; Altarawneh, 2021a,b).

Arrhenius parameters for all the reactions are listed in Table 2. In case of the barrierless reactions, the activation enthalpies are set to zero kcal/mol for the exothermic reactions, whereas, they are assumed to match the enthalpic reaction value if the reaction is endothermic. In the case of the barrierless reaction, there is no energy required to raise the reactants to the transition state energy level to proceed with the reaction which is known as "activation energy". Having that said, when the reaction is exothermic, the activation energy can be considered as zero because the reaction is producing heat and does not require activation energy. On the other hand, when the reaction is barrierless and endothermic, it means that the reaction absorbing heat to produce the reactants but at the same time the reactants do not need a specific amount of energy to be raised to the transition state level and thus, the activation energy can be considered as the same as the enthalpic reaction value. In general, included reactions in the model are categorized into four groups; namely:

- Primary oxidation reactions of PMVE and PEVE initiated by OH radical.
- Bond scissions (either C–C or C–O) for produced perfluorinated adducts
- Oxidation reaction (O₂ addition) and NO/NO₂ reactions with produced peroxy adducts.
- HF elimination reactions.

Fig. 5 portrays molar yields (mol/initial number of PMVE or/PEVE moles) of products, in addition to the associated conversion of the initial reactants. The conversion % (γ) of PMVE as illustrated in Fig. 5a indicates that the PMVE molecule entails almost 50% conversion within 3 h and completely decomposes within 23 h. Thus, it can be noted that, it takes almost a day for the PMVE to be completely removed in atmosphere by OH initiation. This period of time is significantly shorter than predicted for the atmospheric removal of 4:2 fluorotelomer alcohols (FTOHs) (Altarawneh, 2021a,b) at ~ 20 days. The latter value – generally – matches the experimentally reported value for the atmospheric lifetimes of FTOHs in the 20–40 days in the open marine environment (Ellis et al., 2003; Muir et al., 2019). Clearly, the presence of the double bond in HEFs facilitates their atmospheric removal in reference to FTOHs.

Table 2

Arrhenius parameters ($k(T) = AT^n e^{(E_a/(RT))}$) for reactions that participate in the oxidation of PMVE and PEVE initiated by OH radical, fitted in the time range of 280–350 K.

#	Reaction	A (s^{-1} or $cm^3 mol^{-1} s^{-1}$)	n	E_a (cal mol^{-1})
1	$C_2F_5OCF = CF_2$ (PEVE)+ $OH \rightarrow C_4HF_8O_2(M2b)$	1.86×10^4	2.26	-1792
2	$C_4HF_8O_2(M2b)+$ $O_2 \rightarrow C_4HF_8O_4(M3b)$	1.00×10^{13}	0	0
3	$C_4HF_8O_4(M3b)+$ $NO \rightarrow C_4HF_8O_3(M4b)+NO_2$	1.00×10^{13}	0	0
4	$C_4HF_8O_3(M4b) \rightarrow CF_3CF_2OCFO$ (M5b)+ CHF_2O	1.00×10^{13}	0	0
5	$CHF_2O + O_2 \rightarrow CF_2O + HO_2$	1.00×10^{13}	0	0
6	$C_4HF_8O_2(M2b) \rightarrow C_2F_5 + CFOCF_2OH$ (M6)	2.29×10^{11}	0.92	18 728
7	$C_2F_5+O_2 \rightarrow C_2F_5O_2$	1.00×10^{13}	0	0
8	$C_2F_5O_2+NO \rightarrow C_2F_5O + NO_2$	1.00×10^{13}	0	0
9	$C_2F_5O \rightarrow CF_3+CF_2O$	2.52×10^{11}	0.42	5978
10	$CF_3+O_2 \rightarrow CF_3O_2$	1.00×10^{11}	0	0
11	$CF_3O_2+NO \rightarrow CF_3O + NO_2$	1.00×10^{13}	0	0
12	$CF_3O + NO \rightarrow CF_2O + NOF$	1.00×10^{13}	0	0
13	$CF_3O + H_2O \rightarrow CHF_3O + OH$	1.05×10^{11}	0	6518
14	$CHF_3O \rightarrow HF + CF_2O$	7.78×10^{11}	0.4	44 620
15	$C_2HF_3O_2(M6)-HF + CFOCF_2O$	4.80×10^{11}	0.53	44 828
16	$C_2HF_3O_2(M6)+H_2O \rightarrow HF + H_2O + CFOCF_2O$	3.77×10^3	2.21	14 264
17	$C_2F_5OCF = CF_2$ (PEVE)+ $OH \rightarrow C_4HF_8O_2(M8b)$	1.86×10^4	2.26	-1792
18	$C_4HF_8O_2(M8b)+$ $O_2 \rightarrow C_4HF_8O_4(M9b)$	1.00×10^{13}	0	0
19	$C_4HF_8O_4(M9b)+$ $NO \rightarrow C_4HF_8O_3(M10b)+NO_2$	1.00×10^{13}	0	0
20	$C_4HF_8O_3(M10b) \rightarrow$ $C_3HF_6O_2(M11b)+CF_2O$	1.00×10^{13}	0	0
21	$C_3HF_6O_2(M11b)+$ $O_2 \rightarrow C_3CF_2OCFO(M5b)+HO_2$	1.00×10^{13}	0	0
22	$CF_3OCF=CF_2$ (PVME)+ $OH \rightarrow C_3HF_6O_2(M2)$	3.33×10^4	2.29	-1862
23	$C_3HF_6O_2(M2)+O_2 \rightarrow C_3HF_6O_4(M3)$	1.00×10^{13}	0	0
24	$C_3HF_6O_4(M3)+$ $NO \rightarrow C_3HF_6O_3(M4)+NO_2$	1.00×10^{13}	0	0
25	$C_3HF_6O_3(M4) \rightarrow C_2F_4O_2(M5)+$ CHF_2O	1.00×10^{13}	0	0
26	$C_3HF_6O_2(M2) \rightarrow CF_3+ CFOCF_2OH$ (M6)	4.97×10^{11}	0.86	24 209
27	$CF_3OCF=CF_2$ (PVME)+ $OH \rightarrow C_3HF_6O_2(M8)$	3.33×10^4	2.29	-1862
28	$C_3HF_6O_2(M8)+O_2 \rightarrow C_3HF_6O_4(M9)$	1.00×10^{13}	0	0
29	$C_3HF_6O_4(M9)+$ $NO \rightarrow C_3HF_6O_3(M10)+NO_2$	1.00×10^{13}	0	0
30	$C_3HF_6O_3(M10) \rightarrow C_2HF_4O_2(M11)+$ CF_2O	1.00×10^{13}	0	0
31	$C_2HF_4O_2(M11)+O_2 \rightarrow C_2F_4O_2(M5)+$ HO_2	1.00×10^{13}	0	0
32	$C_3HF_6O_2(M2) \rightarrow C_3F_5O_2(M2A)+HF$	1.00×10^{13}	0	0
33	$C_3F_5O_2(M2A)+O_2 \rightarrow C_3F_5O_4(M3A)$	1.00×10^{13}	0	0
34	$C_3F_5O_4(M3A)+$ $NO \rightarrow C_3F_5O_3(M4A)+NO_2$	1.00×10^{13}	0	0
35	$C_3F_5O_3(M4A) \rightarrow CF_3O + CFOCF_2O$ (M7)	3.04×10^{11}	0.67	14 780
36	$C_4HF_8O_2(M2b) \rightarrow C_4F_7O_2(M2B)+HF$	1.00×10^{13}	0	0
37	$C_4F_7O_2(M2B)+O_2 \rightarrow C_4F_7O_4(M3B)$	1.00×10^{13}	0	0
38	$C_4F_7O_4(M3B)+$ $NO \rightarrow C_4F_7O_3(M4B)+NO_2$	1.00×10^{13}	0	0
39	$C_4F_7O_3(M4B) \rightarrow C_2F_5O + CFOCF_2O$ (M7)	1.65×10^{11}	0.69	17 366

The profiles of the main products are illustrated in Fig. 5b. Evident by experiment, Mashino et al. (2000) found that CF_2O , CFOCF_2O and CF_3OCFO are the only detectable carbon bearing products by the Infrared spectra for the OH-initiated oxidation of PMVE. Within ~ 23 h, the highest relative molar yield is 0.64 which is achieved by CF_2O . In addition, Fig. 5b also demonstrates that, CFOCF_2O and CF_3OCFO share the same yield at 0.5. It is worth stating that, the yield remains constant

after ~ 12 h, as shown in Fig. 5b.

As CF_2O appears as a major product from the atmospheric degradation of HFEs, it is important to shed some light on its toxicity and its potential formation form degradation of PFASs in general. CF_2O was also reported as one of the final products from the atmospheric degradation of hexafluoropropene (Saheb and Pourhaghghi, 2014). According to Wang et al. (2020) and Adi and Altarawneh (2022), CF_2O is a primary product from the decomposition of commercial ethylene-alt tetrafluoroethylene copolymers. Also, CF_2O is one of the byproducts from manufacturing of perfluorinated compounds by plasma etching (Xi et al., 2022). CF_2O proves to be highly toxic and hazardous material, and its level of LC50 (Lethal Concentration 50, 4 h) inhaled by rats rests at 270 mg. m^{-3} (Zhang et al., 2019).

Our predicted CF_2O 's relative yield is noticeably lower than the corresponding estimate at 100% reported by Vereecken et al. (2015) for the atmospheric degradation of PMVE. The latter study reported $\sim 40\%$ yield for glycolaldehyde $CFOCF_2OH$ (M6) and $\sim 60\%$ for CF_3OCFO . Also, an experimental analogous molar yield values for CF_2O , CFOCF_2O and CF_3OCFO were recorded to be $\sim 90\%$, $\sim 40\%$ and $\sim 53\%$, respectively under 700 Torr and at 295 K whereas under 10 Torr and at 295 K, they account for $\sim 104\%$, $\sim 69\%$ and $\sim 8\%$, respectively (Mashino et al., 2000). From the later investigation, it can be noted that our obtained yield's values of CFOCF_2O and CF_3OCFO are relatively close to the analogous experimentally values reported at 700 Torr of air diluent and at 295 K. Thus, it is concluded that the product yields of the CFOCF_2O and CF_3OCFO are pressure-dependent (i.e., formation of CFOCF_2O at the expense of CF_3OCFO is preferred at low pressure). Such discrepancy between calculated and experimental yields might be rationalized in terms of a possibility of an equal competition between degradation via HF elimination and collisional stabilization for the excited M2 intermediate (addition reaction of O_2).

The yield of HF is the same as that obtained for CFOCF_2O and CF_3OCFO . A possible attribution for that is that, the pathway for the synthesis of CFOCF_2O also produces HF commencing from the M1 intermediate. The formation of HF was not observed in Mashino et al. (2000) study, which may either be due to loss process, lack of detection sensitivity or its non-formation in air at pressures above 10 Torr (Vereecken et al., 2015). Along the same line of enquiry, theoretical work on the atmospheric decomposition of propyl vinyl ether (PPVE) (Amedro et al., 2015) did not propose pathways for the HF and CFOCF_2O.

Comparing Fig. 5a to c it can be noticed that, the PEVE achieved a $\sim 30\%$ conversion within 3 h and $\sim 97\%$ within 23 h. These two latter values are noticeably lower than the analogous values (50% and 100%) computed for the PMVE molecule within the same period of time (the slope of PMVE curve is steeper than that of PEVE). In other words, it is inferred that dissociation rate of PEVE is lower than that of PMVE and that PEVE requires more than 23 h to reach 100% conversion. Values of lifetimes deduced by kinetic modelling is in accord with that computed from the obtained reaction rate constant for the two molecules; as listed in Table 2. This is also supported by the results shown by Fig. 6 which illustrates that the lifetime of PMVE is ~ 23 h while it is ~ 56 h for PEVE (298.15 K). This may be attributed to the length of carbon chain of the per fluorinated compound, i.e., the longer the carbon chain, the lower the rate of the decomposition reaction and thus, the slower the reaction rate. The concentration of PEVE, CF_2O , CFOCF_2O and CF_3OCFO with respect to time were proposed by (Bunkan et al., 2018). They reported that, $\sim 1.5 \times 10^{13}$ molecule. cm^{-3} PEVE reached after ~ 17 min day. Fig. 6 also shows that the lifetimes of both compounds increase with temperature between 250 and 320 K, reflecting the negative activation barrier obtained for the initial OH addition reaction.

Fig. 5d depicts the time-dependent profiles from the atmospheric oxidation of PEVE. Similar to PMVE, the main products were found to be CF_2O , CFOCF_2O, CF_3CF_2OCFO (M5b) and HF. It is illustrated that, the maximum molar yield of CF_2O is ~ 1.1 (110%) which is higher than the peak yield value achieved from the decomposition of PMVE (64%). In case of PEVE, it takes almost 23 h for CF_2O to reach its maximum molar

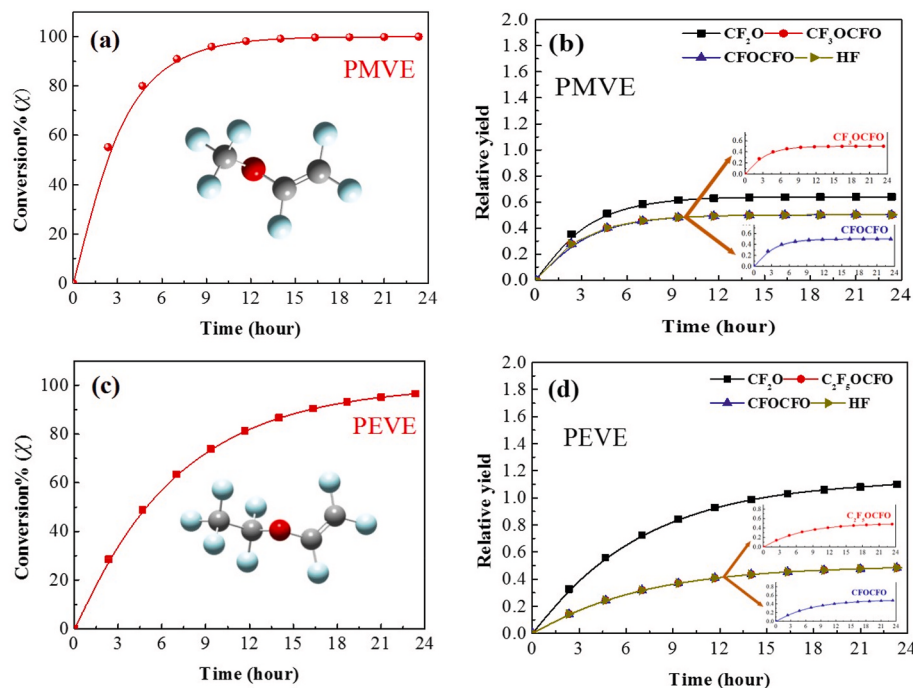


Fig. 5. PMVE conversion profile (a), profiles of main products for PMVE (b), PEVE conversion profile (c), profiles of main products for PEVE (d).

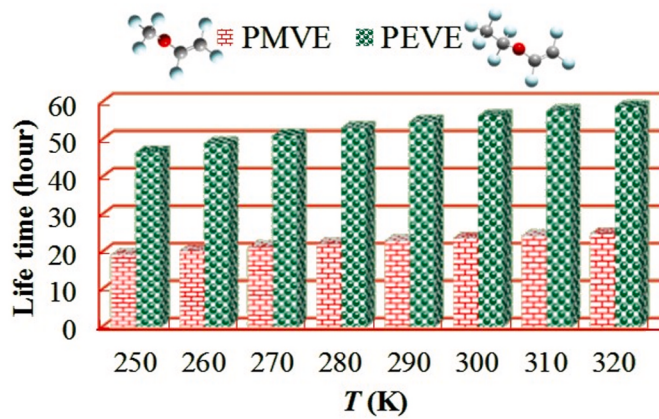


Fig. 6. Lifetime's profile of PMVE and PEVE as a function of temperature.

yield which is longer than the analogous predicted time (~ 19 h) for the same compound to reach its peak value in the case of PMVE (Fig. 5b). In fact, this is an expected behavior since the primary decomposition reaction of PEVE is slower than that of the PMVE as explained above. The predicted molar yield of the CF_2O is somehow lower than that obtained by Hurley et al. (2006) from the oxidation of the $\text{CF}_3\text{CF}_2\text{CHO}$ molecule where the experiment was done using a Pyrex reactor associated with FTIR spectrometer. The later reactor was surrounded by 22 fluorescent black lamps aiming to initiate the experiment photochemically. From the same experiment, it was reported that, in addition to the production of CF_2O , the decomposition reaction proceeds by 50% via the channel that leads to the formation of OH. During photo-oxidation of PEVE initiated by OH, CF_2O was the only detected final products in FTIR (Bunkan et al., 2018). In the same study, a yield of almost 1.5 of the latter compounds was reported within ~ 10 min in the presence of NO which is close to our value, however, at a shorter time.

As portrayed by Fig. 5d, CFOCFO, $\text{CF}_3\text{CF}_2\text{OCFO}$ (M5b) and HF reached their molar yield peak of $\sim 48\%$ after 23 h. The formation of CFOCFO and $\text{CF}_3\text{CF}_2\text{OCFO}$ (M5b) was also detected experimentally by

Bunkan et al. (2018). Comparing the plots of the aforementioned products with that of CF_2O illustrates that, the plot of the later compound displays a non-linear trend and takes a considerable conduction period prior to near constant slope. This serves as an evidence that CF_2O is produced in secondary reactions. If a product is directly formed (or very rapidly formed), its yield will be independent of time, as opposed to a product which is formed in a slow, secondary process. This is also in agreement to analogous findings by Bunkan et al. (2018).

3.3.2. Sensitivity analysis

To precisely comprehend the set of reaction pathways that govern the yield of the major products CF_2O , CFOCFO, CF_3OCFO and $\text{CF}_3\text{CF}_2\text{OCFO}$ (M5b), absolute rate of production analysis was performed at 1260 min and 298.15 K via Chemkin-Pro package for both unsaturated HFEs compounds as illustrated by Fig. 7. Mathematical formulations underpinning sensitivity analysis of chemical kinetics are escribed in detail by Andrea et al. (Saltelli et al., 2005). Numerical implementation rests on the transformation of discrete input factors into continuous uniform distributions across well-defined boundaries of parameters. The seminal work by Turanyi (Turányi, 1997) nicely describes the procedure that underline how calculations of sensitivity analysis are conducted. The procedure computes the output of models as a function of parameters. In this treatment, partial derivatives (expressed as Taylor series expansions) of the output of the model are formulated with respect to the parameters:

$$C_i(t, k + \Delta k) = C_i(t, k) + \sum_{j=1}^m \frac{\partial C_i}{\partial k_j} \Delta k_j + \dots$$

where C represent concentrations of species, k signifies a parameter (i.e., reaction rate constant), and $\frac{\partial C_i}{\partial k_j}$ denotes the concentration sensitivity coefficient.

Fig. 7 a shows that both reaction channels $\text{CF}_3\text{O} + \text{NO} \rightarrow \text{CF}_2\text{O} + \text{NOF}$ and $\text{C}_3\text{HF}_6\text{O}_3(\text{M10}) \rightarrow \text{C}_2\text{HF}_4\text{O}_2(\text{M11}) + \text{CF}_2\text{O}$ are the main reactions that lead to the production of CF_2O from PMVE. However, it appears that, the later reaction accounts for the major production of CF_2O . Along the same line of enquiry, it was reported that CF_2O gas can be produced from the reaction $\text{CF}_3\text{O} + \text{NO} \rightarrow \text{CF}_2\text{O} + \text{NOF}$ under

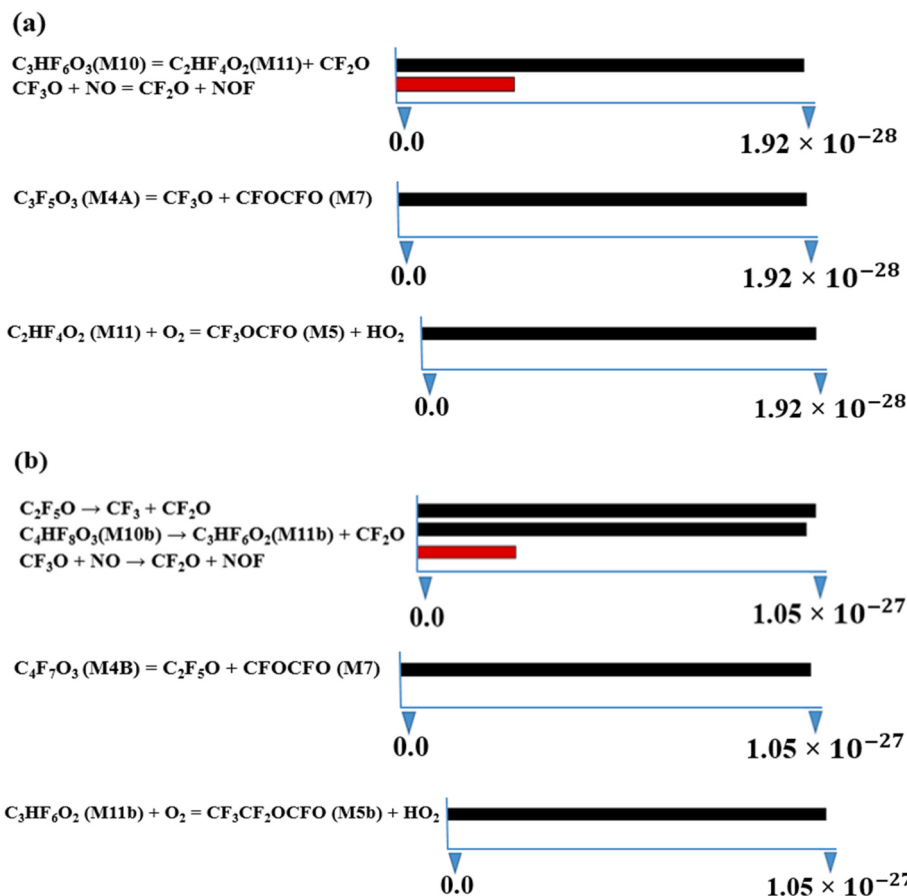


Fig. 7. Absolute rate of production of CF_2O , $CFOCFO$, CF_3OCFO and CF_3CF_2OCFO for PMVE (a) and PEVE (b), computed at 1260 min and 298.15 K.

sufficient concentration of NO (Bunkan et al., 2018). Also, it can be noticed that the production rate of $CFOCFO$, stems from one pathway $C_3F_5O_3(M4A) \rightarrow CF_3O + CFOCFO$ which is in agreement with the finding by Mashino et al. (2000). As shown in Fig. 7, CF_3OCFO , originates from the channel $C_2HF_4O_2(M11) + O_2 \rightarrow CF_3OCFO + HO_2$.

As portrays by Fig. 7 b, there are three suggested pathways for the formation of CF_2O from PEVE, $CF_3O + NO \rightarrow CF_2O + NOF$, $C_4HF_8O_3(M10b) \rightarrow C_3HF_6O_2(M11b) + CF_2O$ and $C_2F_5O \rightarrow CF_3 + CF_2O$. The last two channels account for most of the CF_2O production. Similar to PEVE, the formation of $CFOCFO$ and CF_3OCFO as shown, stem from the same analogous pathways proposed for their formation from PMVE as $C_4F_7O_3 \rightarrow C_2F_5O + CFOCFO$ and $C_3HF_6O_2(M11b) + O_2 \rightarrow CF_3CF_2OCFO + HO_2$, respectively. CF_2O and CF_3OCFO in both compounds arise from OH addition to the inner double bond carbon-carbon atom.

3.3.3. Photochemical ozone creation potential (POCP)

The Photochemical Ozone Creation Potential (POCP) is implemented as an indication of the ability of the material with a given amount to form additional ozone level relative to adding the same amount of ethene (Wuebbles, 1995; Derwent et al., 1996; Wallington et al., 2015, Bhuvaneswari and Senthilkumar, 2020). POCP is considered as one of the most important measurements applied on the ozone protection policy such as the United States Clean Air Act and the Montreal Protocol and its Amendments (Wuebbles, 1995; Jones, 1996). Aiming to estimate the POCP, the following formula was applied, which was suggested by Derwent et al. (1998) and Jenkin (1998):

$$\epsilon^{POCP} = \alpha_1 \times \gamma_s \times \gamma_R^{\beta} (1 - \alpha_2 \times n_c)$$

Where ϵ^{POCP} is the estimated POCP, α_1 , α_2 and β are constants with the

Table 3
Summary of needed values for the POCP calculations.

Parameters	PEVE	PMVE
α_1	111	111
α_2	0.04	0.04
β	0.5	0.5
n_c	4	3
n_B	2	1
M	216	166
k_{OH}	2.48×10^{-13}	5.94×10^{-13}
k_{OH}^{ethene}	8.64×10^{-12}	8.64×10^{-12}
γ_s	0.04	0.03
γ_R	0.09	0.41
POCP	1.18	1.76

values 111, 0.04 and 0.5, respectively (Bhuvaneswari and Senthilkumar, 2020), γ_s and γ_R represents the structure-based and reactivity-based ozone formation indices, respectively and n_c is the number of carbon atoms in the compound. The expressions bellow was used to calculate γ_s and γ_R :

$$\gamma_s = \left(\frac{n_B}{M} \right) \times \left(\frac{28}{6} \right)$$

$$\gamma_R = \left(\frac{k_{OH}}{n_B} \right) \times \left(\frac{6}{k_{OH}^{ethene}} \right)$$

where n_B represents the total number of C-C and C-H bonds in the molecule, M is the molecular weight; k_{OH} is the rate constant for the reaction with OH radicals at 298 K and 760 Torr of air, while k_{OH}^{ethene} is the rate constant for the reaction of ethene with OH radicals at 298 K and

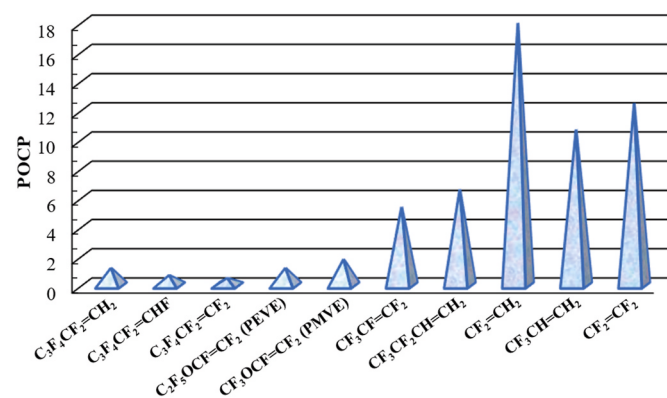


Fig. 8. Photochemical Ozone Creation Potential (POCP) of PMVE, PEVE and other fluorinated compounds.

760 Torr of air (Jenkin, 1998, Bhuvaneswari and Senthilkumar, 2020). Table 3 summarizes the values of the parameters used to calculate the PCOP.

Fig. 8 portrays computed values of POCP for PEVE and PMVE in addition to literature values for other perfluorinated molecules (Wallington et al., 2010; Liu et al., 2016, Bhuvaneswari and Senthilkumar, 2020). As illustrated, while the estimated POCP value of PEVE matches that of 1,2,3,4,5-hexafluorocyclopentene ($\text{C}_3\text{F}_4\text{CF}_2 = \text{CH}_2$) at ~ 1.18 , the PMVE shows a higher value of POCP ~ 1.76 . However, both PEVE and PMVE exhibit insignificant photochemical ozone creation potential (less than 10), which is also relatively lower than some other fluorinated compounds as demonstrated by Fig. 8.

4. Conclusion

In this work, kinetic models were developed along with detailed mechanism pathways to underpin the pathway that govern the PMVE and PEVE atmospheric oxidation initiated by OH. HF elimination leading to the formation of CFOCFO most likely ensues via a water-assisted pathway. Addition of OH to unsaturated carbon atoms in both molecules facilitate attachment of molecular oxygen. The following pathways predominantly originate from peroxy's O abstraction by ambient NO species. In the case of PMVE, it was found that the main end-products are CF_2O with a molar yield of 0.64. CFOCFO, CF_3OCFO and HF entail similar yields of 0.50. Similarly, for PEVE, the major products are found to be CF_2O (with a 1.1 M yield), CFOCFO, $\text{CF}_3\text{CF}_2\text{OCFO}$ and HF (with an equivalent molar yields of 0.48). In reference to experimental measurements, product profiles from the atmospheric oxidation of the two considered HFEs display a pressure-dependent behavior. The lifetime of both PMVE and PEVE molecules increases with temperature, reflecting the negative activation energy for the initial OH addition channels. The analysis of absolute rate of production for PMVE and PEVE portrays important reactions that participate in the formation of the major products and illustrates that the synthesis of most products stem from the addition of OH to the inner carbon-carbon double bond atom. Moreover, the calculated Photochemical Ozone Creation Potentials (POCPs) of PMVE and PEVE revealed that their tendency for the production of tropospheric ozone is negligible. This qualifies them to be promising candidates for CFC replacement with less environmental impact.

CRediT authorship contribution statement

Maissa A. Adi: Formal analysis, Validation, Writing - original draft, Writing - review & editing. **Mohammednoor Altarawneh:** Formal analysis, Funding acquisition, Conceptualization, Methodology, Project administration, Writing - review & editing.

Declaration of competing interest

The authors declare that they have no known competing financial interests or personal relationships that could have appeared to influence the work reported in this paper.

Data availability

Data will be made available on request.

Acknowledgments

This work is supported by a grant from the United Arab Emirates University, UAEU (grant number: 12R174 via the UAEU-AUA Scheme, Asian Universities Alliance). Computations were carried out using the high-performance cluster of the UAEU.

Appendix A. Supplementary data

Supplementary data to this article can be found online at <https://doi.org/10.1016/j.atmosenv.2023.119843>.

References

- Adi, M.A., Altarawneh, M., 2022. Thermal decomposition of heptafluoropropylene-oxide-dimer acid (GenX). Chemosphere 289, 133118.
- Altarawneh, M., 2021a. A chemical kinetic model for the decomposition of perfluorinated sulfonic acids. Chemosphere 263, 128256.
- Altarawneh, M., 2021b. A closer look into the contribution of atmospheric gas-phase pathways in the formation of perfluorocarboxylic acids. Atmos. Pollut. Res. 12 (12), 101255.
- Altarawneh, M., 2022. Temperature-dependent profiles of dioxin-like toxicants from combustion of brominated flame retardants. J. Hazrad. Mater. 422, 126879.
- Altarawneh, M., Carrizo, D., Ziolkowski, A., Kennedy, E.M., Dlugogorski, B.Z., Mackie, J.C., 2009. Pyrolysis of permethrin and formation of precursors of polychlorinated dibenz-p-dioxins and dibenzofurans (PCDD/F) under non-oxidative conditions. Chemosphere 74 (11), 1435–1443.
- Altarawneh, M.K., Dlugogorski, B.Z., Kennedy, E.M., Mackie, J.C., 2013. Rate constants for reactions of ethylbenzene with hydroperoxyl radical. Combust. Flame 160 (1), 9–16.
- Amedro, D., Vereecken, L., Crowley, J., 2015. Kinetics and mechanism of the reaction of perfluoro propyl vinyl ether PPVE, $\text{C}_3\text{F}_7\text{OCH}$ with OH: assessment of its fate in the atmosphere. Phys. Chem. Chem. Phys. 17 (28), 18558–18566.
- Andersen, M.P.S., Nielsen, O.J., 2022. Tropospheric photolysis of CF_3CHO . Atmos. Environ. 272, 118935.
- Bhuvaneswari, R., Senthilkumar, K.J., 2020. First principle studies on the atmospheric oxidation of HFC-C143e initiated by the OH radical. New J. Chem. 44 (5), 2070–2082.
- Brudnik, K., Jodkowski, J.T., Sarzyński, D., Nowek, A., 2011. Mechanism of the gas-phase decomposition of trifluoro-, trichloro-, and tribromomethanols in the presence of hydrogen halides. J. Mol. Model. 17 (9), 2395–2409.
- Brudnik, K., Wójcik-Pastuszka, D., Jodkowski, J.T., Leszczynski, J., 2008. Theoretical study of the kinetics and mechanism of the decomposition of trifluoromethanol, trichloromethanol, and tribromomethanol in the gas phase. J. Mol. Model. 14 (12), 1159–1172.
- Bunkan, A.J.C., Srinivasulu, G., Amedro, D., Vereecken, L., Wallington, T., Crowley, J., 2018. Products and mechanism of the OH-initiated photo-oxidation of perfluoro ethyl vinyl ether, $\text{C}_2\text{F}_5\text{OCFCF}_2$. Phys. Chem. Chem. Phys. 20 (16), 11306–11316.
- Buszek, R.J., Francisco, J.S., 2009. The gas-phase decomposition of CF_3OH with water: a radical-catalyzed mechanism. J. Phys. Chem. A 113 (18), 5333–5337.
- Canneaux, S., Bohr, F., Henon, E., 2014. KiSTheLP: a program to predict thermodynamic properties and rate constants from quantum chemistry results. J. Comput. Chem. 35 (1), 82–93.
- Cheng, B., Alapaty, K., Zartarian, V., Poulakos, A., Strynar, M., Buckley, T., 2021. Per- and polyfluoroalkyl substances exposure science: current knowledge, information needs, future directions. Int. J. Environ. Sci. Technol. 1–16.
- Cousins, I.T., DeWitt, J.C., Glüge, J., Goldenman, G., Herzke, D., Lohmann, R., Ng, C.A., Scheringer, M., Wang, Z., 2020. The high persistence of PFAS is sufficient for their management as a chemical class. Environ. Sci.: Process. Impacts 22 (12), 2307–2312.
- Derwent, R., Jenkin, M., Saunders, S.J.A.E., 1996. Photochemical ozone creation potentials for a large number of reactive hydrocarbons under European conditions. Atmos. Environ. 30 (2), 181–199.
- Derwent, R.G., Jenkin, M.E., Saunders, S.M., Pilling, M.J., 1998. Photochemical ozone creation potentials for organic compounds in northwest Europe calculated with a master chemical mechanism. Atmos. Environ. 32 (14–15), 2429–2441.
- Ding, X., Song, X., Chen, X., Ding, D., Xu, C., Chen, H., 2022. Degradation and mechanism of hexafluoropropylene oxide dimer acid by thermally activated persulfate in aqueous solutions. Chemosphere 286, 131720.

- Ellis, D., Martin, J., Mabury, S., Hurley, M., Sulbaek Andersen, M., Wallington, T., 2003. Atmospheric lifetime of fluorotelomer alcohols. *Environ. Sci. Technol.* 37 (17), 3816–3820.
- Ellis, D.A., Martin, J.W., De Silva, A.O., Mabury, S.A., Hurley, M.D., Sulbaek Andersen, M.P., Wallington, T.J., 2004. Degradation of fluorotelomer alcohols: a likely atmospheric source of perfluorinated carboxylic acids. *Environ. Sci. Technol.* 38 (12), 3316–3321.
- Frisch, M.J., Trucks, G.W., Schlegel, H.B., Scuseria, G.E., Robb, M.A., Cheeseman, J.R., Scalmani, G., Barone, V., Petersson, G.A., Nakatsuji, H., Li, X., Caricato, M., Marenich, A.V., Bloino, J., Janesko, B.G., Gomperts, R., Mennucci, B., Hratchian, H.P., Ortiz, J.V., Izmaylov, A.F., Sonnenberg, J.L., Williams Ding, F., Lipparini, F., Egidi, F., Goings, J., Peng, B., Petrone, A., Henderson, T., Ranasinghe, D., Zakrzewski, V.G., Gao, J., Rega, N., Zheng, G., Liang, W., Hada, M., Ehara, M., Toyota, K., Fukuda, R., Hasegawa, J., Ishida, M., Nakajima, T., Honda, Y., Kitao, O., Nakai, H., Vreven, T., Throssell, K., Montgomery Jr., J.A., Peralta, J.E., Ogliaro, F., Bearpark, M.J., Heyd, J.J., Brothers, E.N., Kudin, K.N., Staroverov, V.N., Keith, T.A., Kobayashi, R., Normand, J., Raghavachari, K., Rendell, A.P., Burant, J.C., Iyengar, S.S., Tomasi, J., Cossi, M., Millam, J.M., Klene, M., Adamo, C., Cammi, R., Ochterski, J.W., Martin, R.L., Morokuma, K., Farkas, O., Foresman, J.B., Fox, D.J., 2016. Gaussian 16. Rev. C.01, Wallingford, CT.
- Giessing, A., Feilberg, A., Mogelberg, T., Sehested, J., Bilde, M., Wallington, T.J., Nielsen, J., 1996. Atmospheric chemistry of HFC-227ca: spectrokinetic investigation of the $\text{CF}_3\text{CF}_2\text{CF}_2\text{O}_2$ radical, its reactions with NO and NO_2 , and the atmospheric fate of the $\text{CF}_3\text{CF}_2\text{CF}_2\text{O}$ radical. *J. Phys. Chem.* 100 (16), 6572–6579.
- Glüge, J., Scheringer, M., Cousins, I.T., DeWitt, J.C., Goldeman, G., Herzke, D., Lohmann, R., Ng, C.A., Trier, X., Wang, Z., 2020. An overview of the uses of per-and polyfluoroalkyl substances (PFAS). *Environ. Sci.: Process. Impacts* 22 (12), 2345–2373.
- Gonu, S., Bunkan, A.J.C., Amedro, D., Crowley, J., 2018. Absolute and relative-rate measurement of the rate coefficient for reaction of perfluoro ethyl vinyl ether ($\text{C}_2\text{F}_5\text{OCF}=\text{CF}_2$) with OH. *Phys. Chem. Chem. Phys.* 20 (5), 3761–3767.
- Good, D.A., Francisco, J.S., 2003. Atmospheric chemistry of alternative fuels and alternative chlorofluorocarbons. *Chem. Rev.* 103 (12), 4999–5024.
- Holland, R., Khan, M.A.H., Driscoll, I., Chhantyal-Pun, R., Derwent, R.G., Taatjes, C.A., Orr-Ewing, A.J., Percival, C.J., Shallcross, D.E., 2021. Investigation of the production of trifluoroacetic acid from two halocarbons, HFC-134a and HFO-1234yf and its fates using a global three-dimensional chemical transport model. *ACS Earth and Space Chem.* 5 (4), 849–857.
- Hurley, M., Ball, J., Wallington, T., Sulbaek Andersen, M., Nielsen, O., Ellis, D., Martin, J., Mabury, S., 2006. Atmospheric chemistry of $n\text{C}_x\text{F}_{2x+1}\text{CHO}$ ($x=1, 2, 3, 4$): fate of $n\text{C}_x\text{F}_{2x+1}\text{C}$ (O) radicals. *J. Phys. Chem. A* 110 (45), 12443–12447.
- Jenkin, M., 1998. Photochemical Ozone and PAN Creation Potentials: Rationalisation and Methods of Estimation, Report AEAT-4182/2015/003. National Environmental Technology Centre, AEA Technology plc Culham.
- Jensen, N.R., Hanson, D.R., Howard, C.J., 1994. Temperature dependence of the gas phase reactions of CF_3O with CH_4 and NO . *J. Phys. Chem.* 98 (34), 8574–8579.
- Jones, T.T., 1996. Implementation of the Montreal Protocol: barriers, constraints and opportunities. *J. Envtl. Law.* 3, 813.
- Jovell, D., Gonzalez-Olmos, R., Llovel, F., 2022. A computational drop-in assessment of hydrofluoroethers in Organic Rankine Cycles. *Energy* 254, 124319.
- Kelly, C., Sidebottom, H.W., Treacy, J., Nielsen, O.J., 1994. Reactions of CF_3O radicals with selected alkenes and aromatics under atmospheric conditions. *Chem. Phys. Lett.* 218 (1–2), 29–33.
- Khan, M.Y., So, S., da Silva, G., 2020. Decomposition kinetics of perfluorinated sulfonic acids. *Chemosphere* 238, 124615.
- Kondo, Y., Ishikawa, K., Hayashi, T., Miyawaki, Y., Takeda, K., Kondo, H., Sekine, M., Hori, M., 2015. CF_3^+ fragmentation by electron impact ionization of perfluoropropyl-vinyl-ethers, $\text{C}_5\text{F}_{10}\text{O}$, in gas phase. *Jpn. J. Appl. Phys.* 54 (4), 040301.
- Li, Z., Francisco, J., 1991. Laser-induced fluorescence spectroscopic study of the transition of trifluoromethoxy radical. *Chem. Phys. Lett.* 186 (4–5), 336–342.
- Li, Z., Tao, Z., Naik, V., Good, D.A., Hansen, J.C., Jeong, G.R., Francisco, J.S., Jain, A.K., Weubbles, D.J., 2000. Global warming potential assessment for $\text{CF}_3\text{OCF}=\text{CF}_2$. *J. Geophys. Res. Atmos.* 105 (D3), 4019–4029.
- Lily, M., Baidya, B., Wang, W., Liu, F., Chandra, A.K., 2020. Atmospheric chemistry of $\text{CHF}_2\text{CF}_2\text{OCH}_2\text{CF}_3$: reactions with Cl atoms, fate of $\text{CHF}_2\text{CF}_2\text{O}\bullet$ HCF_3 radical, formation of OH radical and Crieger Intermediate. *Atmos. Environ.* 242, 117805.
- Lily, M., Hynniewita, S., Muthiah, B., Wang, W., Chandra, A.K., Liu, F., 2021. Quantum chemical insights into the atmospheric reactions of $\text{CH}_2\text{FC}_2\text{OH}$ with OH radical, fate of $\text{CH}_2\text{FC}\bullet$ HOH radical and ozone formation potential. *Atmos. Environ.* 249, 118247.
- Liu, D., Qin, S., Li, W., Zhang, D., Guo, Z.J.T., 2016. Atmospheric chemistry of 1-H-heptafluorocyclopentene (cyc- $\text{CF}_2\text{CF}_2\text{CF}_2\text{CFCF}_3$): rate constant, products, and mechanism of gas-phase reactions with OH radicals, IR absorption spectrum, photochemical ozone creation potential, and global warming potential. *J. Phys. Chem. A* 120 (48), 9557–9563.
- Long, B., Tan, X.-f., Ren, D.-s., Zhang, W.-j., 2010. Theoretical studies on energetics and mechanisms of the decomposition of CF_3OH . *Chem. Phys. Lett.* 492 (4–6), 214–219.
- Mashino, M., Kawasaki, M., Wallington, T., Hurley, M., 2000. Atmospheric degradation of $\text{CF}_3\text{OCFCF}_2$: kinetics and mechanism of its reaction with OH radicals and Cl atoms. *J. Phys. Chem. A* 104 (13), 2925–2930.
- McDonough, C.A., Li, W., Bischel, H.N., De Silva, A.O., DeWitt, J.C., 2022. Widening the lens on PFASs: direct human exposure to perfluoroalkyl acid precursors (pre-PFAs). *Environ. Sci. Technol.* 56, 6004–6013.
- Mokrushin, V., Bedanov, V., Tsang, W., Zachariah, M., Knyazev, V., ChemRate, V., 2002. 1.19. NIST, Gaithersburg, MD.
- Montgomery Jr., J.A., Frisch, M.J., Ochterski, J.W., Petersson, G.A., 2000. A complete basis set model chemistry. VII. Use of the minimum population localization method. *J. Chem. Phys.* 112 (15), 6532–6542.
- Muir, D., Bossi, R., Carlsson, P., Evans, M., De Silva, A., Halsall, C., Rauert, C., Herzke, D., Hung, H., Letcher, R., 2019. Levels and trends of poly-and perfluoroalkyl substances in the Arctic environment—An update. *Emerg. Contam.* 5, 240–271.
- Nguyen, M.T., Matus, M.H., Ngan, V.T., Haiges, R., Christe, K.O., Dixon, D.A., 2008. Energetics and mechanism of the decomposition of trifluoromethanol. *J. Phys. Chem. A* 112 (6), 1298–1312.
- Orkin, V.L., Khamaganov, V.G., Martynova, L.E., Kurylo, M.J., 2011. High-accuracy measurements of $\text{OH}\bullet$ reaction rate constants and IR and UV absorption spectra: ethanol and partially fluorinated ethyl alcohols. *J. Phys. Chem. A* 115 (31), 8656–8668.
- Purnell Jr., D.L., Bozzelli, J.W., 2018. Thermochemical properties: enthalpy, entropy, and heat capacity of $\text{C}_2\text{-C}_3$ fluorinated aldehydes, radicals and fluorocarbon group additivity. *J. Phys. Chem. A* 123 (3), 650–665.
- Razmgar, K., Altarawneh, M., Oluwuye, I., Senayake, G., 2022. Selective hydrogenation of 1,3-butadiene over ceria catalyst: a molecular insight. *Mol. Catal.* 524, 112331.
- Sahab, V., Pourhaghghi, N.Y., 2014. Theoretical kinetics studies on the Reaction of $\text{CF}_3\text{CF}=\text{CF}_2$ with hydroxyl radical. *J. Phys. Chem. A* 118 (43), 9941–9950.
- Saltelli, A., Ratto, M., Tarantola, S., Campolongo, F., 2005. Sensitivity analysis for chemical models. *Chem. Rev.* 105 (7), 2811–2828.
- Shohrat, A., Zhang, M., Hu, H., Yang, X., Liu, L., Huang, H., 2022. Mechanism study on CO_2 capture by ionic liquids made from TFA blended with MEA and MDEA. *Int. J. Greenh. Gas Control* 119, 103709.
- Somnitz, H., Zellner, R., 2001. Theoretical studies of the thermal and chemically activated decomposition of $\text{CF}_3\text{CY}_2\text{O}$ ($\text{Y}=\text{F}, \text{H}$) radicals. *Phys. Chem. Chem. Phys.* 3 (12), 2352–2364.
- Srinivasulu, G., Bunkan, A., Amedro, D., Crowley, J., 2018. Absolute and relative-rate measurement of the rate coefficient for reaction of perfluoro ethyl vinyl ether ($\text{C}_2\text{F}_5\text{OCFCF}_2$) with OH. *Phys. Chem. Chem. Phys.* 20 (5), 3761–3767.
- Sun, X., He, M., Zhang, Q., Wang, W., Jalbout, A.F., 2008. Quantum chemical study on the atmospheric photooxidation of methyl vinyl ether (MVE). *J. Mol. Struct.: THEOCHEM* 868 (1–3), 87–93.
- Sunderland, E.M., Hu, X.C., Dassuncao, C., Tokranov, A.K., Wagner, C.C., Allen, J.G., 2019. A review of the pathways of human exposure to poly-and perfluoroalkyl substances (PFASs) and present understanding of health effects. *J. Expo. Sci. Environ. Epidemiol.* 29 (2), 131–147.
- Thackray, C.P., Selin, N.E., 2017. Uncertainty and variability in atmospheric formation of PCFs from fluorotelomer precursors. *Physics Atmos. Chem.* 17 (7), 4585–4597.
- Thackray, C.P., Selin, N.E., Young, C.J., 2020. A global atmospheric chemistry model for the fate and transport of PCFs and their precursors. *Environ. Sci.: Process. Impacts* 22 (2), 285–293.
- Turányi, T., 1997. Applications of sensitivity analysis to combustion chemistry. *Reliab. Eng. Syst.* 57 (1), 41–48.
- Turnipseed, A.A., Barone, S.B., Jensen, N.R., Hanson, D., Howard, C.J., Ravishankara, A., 1995. Kinetics of the reactions of CF_3O radicals with CO and H_2O . *J. Phys. Chem.* 99 (16), 6000–6009.
- Vereecken, L., Crowley, J., Amedro, D., 2015. Theoretical study of the OH-initiated atmospheric oxidation mechanism of perfluoro methyl vinyl ether, $\text{CF}_3\text{OCFCF}_2$. *Phys. Chem. Chem. Phys.* 17 (43), 28697–28704.
- Wallington, T., Andersen, M.S., Nielsen, O., 2010. Estimated photochemical ozone creation potentials (POCPs) of CF_3CFCH_2 (HFO-1234yf) and related hydrofluoroolefins (HFOs). *Atmos. Environ.* 44 (11), 1478–1481.
- Wallington, T., Andersen, M.S., Nielsen, O., 2015. Atmospheric chemistry of short-chain haloolefins: photochemical ozone creation potentials (POCPs), global warming potentials (GWPs), and ozone depletion potentials (ODPs). *Chemosphere* 129, 135–141.
- Wallington, T.J., Ball, J.C., 1995. Atmospheric chemistry of CF_3O radicals: reaction with CH_4 , CD_4 , CH_3F , CF_3H , ^{13}CO , $\text{C}_2\text{H}_5\text{F}$, C_2D_6 , C_2H_6 , CH_3OH , $i\text{-C}_4\text{H}_8$, and C_2H_2 . *J. Phys. Chem.* 99 (10), 3201–3205.
- Wang, C., Chen, Q., Guo, X., Li, Y., Zhang, J., Liu, G., Feng, W., 2020. On thermal decomposition kinetics of poly(ethylene-alt-tetrafluoroethylene) using an autocatalytic model. *J. Fluor. Chem.* 240, 109656.
- Wang, S., Lin, X., Li, Q., Liu, C., Li, Y., Wang, X., 2022. Neutral and ionizable per-and polyfluoroalkyl substances in the urban atmosphere: occurrence, sources and transport. *Sci. Total Environ.* 823, 153794.
- Weubbles, D.J., 1995. Weighing functions for ozone depletion and greenhouse gas effects on climate. *Annu. Rev. Energy Environ.* 20 (1), 45–70.
- Xi, W., Guo, L., Liu, D., Zhou, R., Wang, Z., Wang, W., Liu, Z., Wang, X., Ostrikov, K.K., Rong, M., 2022. Upcycle hazard against other hazard: toxic fluorides from plasma fluoropolymer etching turn novel microbial disinfectants. *J. Hazrad. Mater.* 424, 127658.
- Yu, Y., Xu, H., Yao, B., Pu, J., Jiang, Y., Ma, Q., Fang, X., O'Doherty, S., Chen, L., He, J., 2022. Estimate of hydrochlorofluorocarbon emissions during 2011–2018 in the yangtze river delta, China. *Environ. Pollut.* 15, 119517.
- Zhang, Y., Zhang, X., Li, Y., Li, Y., Chen, Q., Zhang, G., Xiao, S., Tang, J., 2019. Effect of oxygen on power frequency breakdown voltage and decomposition characteristics of the C_6F_{10} O/N 2/O2 gas mixture. *RSC Adv.* 9 (33), 18963–18970.
- Zhao, Y., Truhlar, D.G., 2008. The M06 suite of density functionals for main group thermochemistry, thermochemical kinetics, noncovalent interactions, excited states, and transition elements: two new functionals and systematic testing of four M06-class functionals and 12 other functionals. *Theor. Chem. Acc.* 120 (1), 215–241.
- Zharov, A., Nikolaeva, O., 2010. Kinetic regularities and mechanism of polymerization of perfluoromethylvinyl ether at high pressures. *Russ. J. Phys. Chem.* 4 (5), 839–845.